J. Fluid Mech. (1988), *vol.* 190, *pp.* 451–469
Printed in Great Britain

Interpretation of shadowgraph patterns in Rayleigh–Bénard convection

By D. R. JENKINS
CSIRO Division of Mathematics and Statistics, PO Box 218, Lindfield NSW 2070, Australia

(Received 22 October 1986 and in revised form 2 November 1987)

The relationship between observations of cellular Rayleigh–Bénard convection using shadowgraphs and theoretical expressions for convection planforms is considered. We determine the shadowgraphs that ought to be observed if the convection is as given by theoretical expressions for roll, square or hexagonal planforms and compare them with actual experiments. Expressions for the planforms derived from linear theory, valid for low supercritical Rayleigh number, produce unambiguous shadowgraphs consisting of cells bounded by bright lines, which correspond to surfaces through which no fluid flows and on which the vertical component of velocity is directed downwards. Dark spots at the centre of cells, indicating regions of hot, rising fluid, are not accounted for by linear theory, but can be produced by adding higher-order terms, predominantly due to the temperature dependence of a material property of the fluid, such as its viscosity.

1. Introduction

There has been a number of planform studies of Rayleigh–Bénard convection over the past 20 years. On the theoretical side, interest has been in the competition between the roll, square and hexagonal planforms for steady convection. On the experimental side, convection planforms are often observed using a shadowgraph, which is a two-dimensional image of the planform derived from a three-dimensional field. The shadowgraph technique relies upon the variation of the refractive index of a fluid with its density, and hence its temperature. The aim of this paper is to relate observed shadowgraph patterns to theoretical representations of particular planforms.

When referring to cellular convection, many authors quote the paper of Stuart (1964), which appears to be the currently accepted view of the relationship between theory and experiment. In that paper, Stuart points out the differences in form of the hexagonal cell and the so-called square and rectangular cells. His conclusion is that a square (or rectangular) cell of the generally accepted form, derived from linear theory, would not be observed in experiments. His reasons are based upon the assumption that the observed cellular boundaries are surfaces through which no fluid passes and on which the vertical component of velocity has the same sign everywhere. There is no unambiguous way of obtaining such surfaces for the square or rectangular solutions. We show that the shadowgraph technique does produce an unambiguous pattern for the square solution, as indeed it does for the hexagonal and roll solutions, and that the cell boundaries are in fact the surfaces on which fluid is moving downwards. Moreover, we assert that the shadowgraph patterns obtained for convection at highly supercritical Rayleigh numbers are related to the roll, square

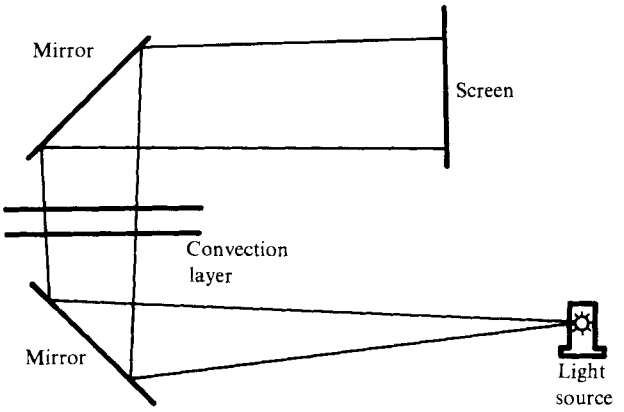

FIGURE 1. Schematic of the shadowgraph process (from Busse 1978).

and hexagonal solutions derived from linear theory, but are modified by higher-order terms.

Experimental work by Koschmieder (1966), Whitehead & Parsons (1978), White (1982), Oliver & Booker (1983) and Le Gal Pocheau & Croquette (1985) has shown that steady square-cell convection is physically possible, and theoretical studies have shown that it is the preferred solution under certain conditions (Busse & Riahi 1980; Proctor 1981; Jenkins & Proctor 1984; Busse & Frick 1985; Jenkins 1987). However, there has been some discussion about the nature of the square cell observed and its relation to theory. Instead of the 'chequerboard' pattern conventionally thought of as representing square-planform convection, shadowgraphs of the observed cells exhibited hot regions (which appear as dark spots) at the centre of each square, and cold regions (bright lines) along the edges. Drobyshevski & Yuferev (1974) proposed an alternative form for square-cell convection which has the same topology as the hexagonal planform, and which has been used in recent studies (e.g. Arter 1985; Schmidt, Simon & Weiss 1985). It has been asserted (Swift 1984) that the lack of vertical symmetry due to the temperature-dependent viscosity leads to the different type of square cell. We show that the observed patterns can be accounted for by careful consideration of the shadowgraph technique. At the same time, we examine the shadowgraph pattern produced by roll and hexagonal convection.

It has been stated that a shadowgraph represents the vertically averaged temperature of the fluid layer (Busse 1978; Arter 1985). Because the temperature field takes the same form as the vertical velocity of the fluid (in the linear approximation), a shadowgraph is also interpreted as indicating regions of rising and sinking fluid. In fact, a shadowgraph is produced by deflection of light rays passed through the fluid layer and subsequently focused onto a screen (see figure 1). The effect of deflection and focusing is to produce a pattern which is related to the temperature field, but is not actually a vertical average.

In the following section we present theoretical descriptions of convection planforms, and a model of the shadowgraph technique is proposed in §3. In §4 we present pictures depicting theoretical shadowgraphs derived from the model equations and relate them to actual experiments. Finally, we summarize the results and discuss their implications.

It is believed that the work shown here is the first attempt to derive shadowgraph patterns from theoretical expressions for three-dimensional thermal convection.

Houseman (1981) has used a similar procedure to investigate light-intensity variations caused by two-dimensional convection. He used numerical solutions of a thermal-convection problem at high Rayleigh numbers as input to his model and found good agreement with measurements of light intensity in the corresponding experimental configuration.

2. Convection planforms

The onset of Rayleigh–Bénard convection represents a deviation from the basic state of no fluid motion and a linear temperature profile in the vertical direction. In an appropriately scaled Cartesian coordinate system, the temperature T at any point in the layer may be written as

$$T - T_0 = -z + T'(x, y, z, t), \tag{2.1}$$

where T_0 is a reference temperature, z is the vertical coordinate, T' is the deviation from the basic state and t is time. For convection sufficiently close to onset, T' and the fluid velocity may be expanded in terms of a small parameter ϵ, in the form

$$T' = \epsilon T_1 + \epsilon^2 T_2 + \epsilon^3 T_3 + \ldots, \tag{2.2}$$

and the expansions substituted into the appropriate nonlinear equations for the conservation of heat, mass and momentum. At first order in ϵ, the equations are linear, and separable in the horizontal coordinates, so we can write

$$\begin{bmatrix} T_1 \\ w_1 \end{bmatrix} = f(x, y) \begin{bmatrix} g(z) \\ h(z) \end{bmatrix}, \tag{2.3}$$

where w_1 is the vertical component of velocity at first order. The function f is the planform function, and it satisfies the Helmholtz equation

$$f_{xx} + f_{yy} = -a^2 f, \tag{2.4}$$

where the subscripts denote differentiation, and a^2 denotes the sum of the squares of the horizontal wavenumbers. Equation (2.4) has an infinite number of solutions, and the actual solution that is observed in a given situation cannot be determined from linear theory. Of particular interest among the solutions of (2.4) are the following 'regular' solutions:

$$f = \cos ax, \tag{2.5}$$

$$f = \cos ax + \cos ay, \tag{2.6}$$

$$f = \cos \tfrac{1}{2}(\sqrt{3}ax + ay) + \cos \tfrac{1}{2}(\sqrt{3}ax - ay) + \cos ay, \tag{2.7}$$

which represent roll, square and hexagonal planforms, respectively. These are steady solutions, and which of them is realized in an experiment is determined by factors such as boundary conditions and properties of the convecting fluid. At second and higher orders in the expansion, higher-order approximations to the temperature and velocity field are obtained.

A particularly interesting situation is the one in which the boundaries of the convection layer are very poor conductors of heat. Then the horizontal lengthscale is so large that an expansion scheme can be developed which separates the vertical and horizontal coordinates. This problem has been considered by Chapman &

Proctor (1980), Proctor (1981), Gertsberg & Sivashinsky (1981) and Depassier & Spiegel (1982). The following nonlinear equation for f can be derived:

$$f_t = -A(R-R_c)\nabla_H^2 f - B\nabla_H^4 f + C\nabla_H\cdot(|\nabla_H f|^2\nabla_H f) + \xi\nabla_H\cdot(f\nabla_H f) - f, \quad (2.8)$$

where A, B and C are constants, R is the Rayleigh number and R_c is the critical Rayleigh number for perfectly insulating boundaries, ∇_H is the horizontal gradient and ξ is an $O(1)$ parameter which is a measure of the temperature dependence of viscosity, defined by

$$\mu = \mu_0[1-\epsilon^2\xi(T-T_0)].$$

Here μ_0 and T_0 are the viscosity and temperature, respectively, at the centre of the fluid layer and ϵ is the expansion parameter, which depends on the (small) thermal conductivity of the boundaries of the layer.

We are only interested in steady convection, so we set the left-hand side of (2.8) to zero. Expanding f in terms of a small parameter δ as

$$f = \delta f_1 + \delta^2 f_2 + \delta^3 f_3 + \ldots, \quad (2.9)$$

and substituting into (2.8) we obtain a series of linear problems, which yield the solutions

$$f_2 = -\tfrac{1}{9}\xi(P^2\cos 2ax + Q^2\cos 2ay) - 2\xi PQ\cos ax\cos ay, \quad (2.10a)$$

$$f_3 = p_1(P^3\cos 3ax + Q^3\cos 3ay) + p_2(PQ^2\cos ax\cos 2ay + P^2Q\cos 2ax\cos ay), \quad (2.10b)$$

where $P = Q = 1$ for a square planform and $P = 1$, $Q = 0$ for a roll planform. The coefficients p_1 and p_2 are, for rigid boundaries,

$$p_1 = \tfrac{1}{128}[\tfrac{15}{7} + \xi^2], \quad p_2 = \tfrac{1}{16}[\tfrac{5}{7} + \tfrac{14}{9}\xi^2]. \quad (2.11)$$

For a hexagonal planform a similar expansion yields

$$f_2 = -\tfrac{1}{9}\xi[\cos(\sqrt{3}ax + ay) + \cos(\sqrt{3}ax - ay) + \cos 2ay] - \tfrac{1}{4}\xi[\cos(\sqrt{3}ax) + \cos\tfrac{1}{2}(\sqrt{3}ax + 3ay) + \cos\tfrac{1}{2}(\sqrt{3}ax - 3ay)], \quad (2.12a)$$

$$f_3 = p_1[\cos 3ay + \cos\tfrac{1}{2}(3\sqrt{3}ax + 3ay) + \cos\tfrac{1}{2}(3\sqrt{3}ax - 3ay)] + p_3[\cos(\sqrt{3}ax + 2ay) + \cos(\sqrt{3}ax - 2ay) + \cos\tfrac{1}{2}(\sqrt{3}ax + 5ay) + \cos\tfrac{1}{2}(\sqrt{3}ax - 5ay) + \cos\tfrac{1}{2}(3\sqrt{3}ax + ay) + \cos\tfrac{1}{2}(3\sqrt{3}ax - ay)], \quad (2.12b)$$

where

$$p_3 = \tfrac{1}{32}[\tfrac{10}{7} + \tfrac{91}{81}\xi^2]. \quad (2.13)$$

The expressions for f_1 are the planforms given in (2.5)–(2.7).

The advantage of the poorly conducting-boundary solution is that the algebra involved is simple enough to allow the expansion to be carried to third order. The expressions for the various planforms will be used in the remainder of the paper as prototypes of roll, square and hexagonal convection planforms in order to determine the shadowgraphs that they produce.

3. Shadowgraph model

Consider the configuration shown in figure 2. Parallel vertical light rays enter a horizontal layer of fluid whose refractive index $n(x, y, z)$ varies throughout the fluid. The refractive index of a fluid varies with the fluid temperature approximately as

$$n = n_0 + n_1(T - T_0).$$

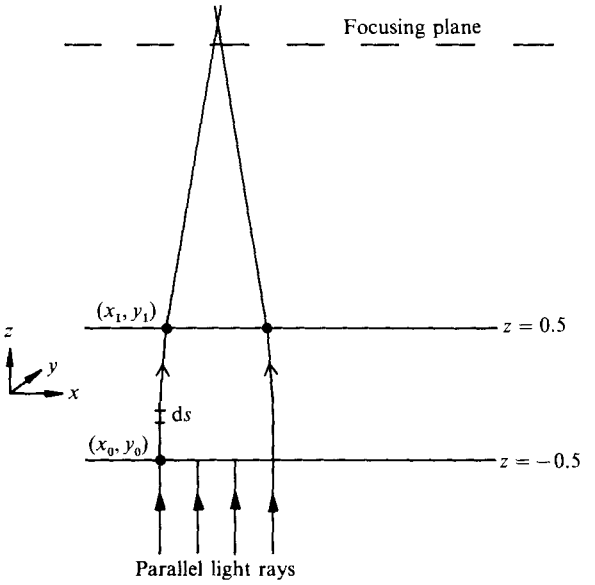

FIGURE 2. Configuration for determination of the model equations.

For most fluids, n_1 is negative, so the refractive index decreases with increasing temperature. Consequently, light rays bend towards colder fluid regions. Houseman (1981) gave the following values for silicone oil:

$$n_0 = 1.4135, \quad n_1 = -3.8122 \times 10^{-4}\ \mathrm{K}^{-1}$$

which is typical of experimental fluids. Thus a temperature variation of 50 K in an experiment using silicone oil would result in a maximum variation of only 0.02 in refractive index.

The path through the fluid layer is short, so the horizontal position (x_1, y_1) at which the light ray exits the layer will differ only slightly from (x_0, y_0). However, two rays entering parallel, but in different parts of the layer, will exit with small deviations from parallel. Once the rays exit the layer, they travel through a medium with constant refractive index (i.e. air), so their trajectories are straight lines. The deflections caused by the fluid layer lead to the rays converging in some areas and diverging in others. The converging rays will focus, i.e. converge to a point, at some height above the layer, which corresponds to the screen position in the experimental set-up (figure 1).

A simple shadowgraph model can be derived by assuming that the deflection of a ray through the fluid is negligible, so a ray entering the layer at (x_0, y_0) also exits at (x_0, y_0). However, the variation in refractive index due to thermal convection causes the ray to exit the layer bent in the direction of the gradient of f. Then at the top of the layer we have

$$x' = -Kf_x, \quad y' = -Kf_y, \tag{3.1a,b}$$

where the constant K is positive, since rays deflect towards colder regions of fluid. This is the paraxial approximation, and has been shown by Ryrie (1987) to be valid when the variations in refractive index are small and the fluid layer is thin. We focus the rays at a height z_F by integrating (3.1) to give

$$x(z_F) = x_0 - Kf_x z_F, \quad y(z_F) = y_0 - Kf_y z_F. \tag{3.2a,b}$$

The Jacobian

$$J(z) = \frac{\partial(x(z), y(z))}{\partial(x_0, y_0)}$$

gives a measure of the area change along a ray trajectory, and consequently light intensity is proportional to the inverse of the Jacobian. The Jacobian at the focusing level is

$$J = 1 - Kz_{\mathrm{F}}(f_{xx} + f_{yy}) + K^2 z_{\mathrm{F}}^2 (f_{xx} f_{yy} - f_{xy}^2), \tag{3.3}$$

where the derivatives in (3.2), (3.3) are evaluated at (x_0, y_0). The value of K depends on the parameter n_1 and the Rayleigh number R, so it determines the height at which focusing occurs.

A more detailed model of the deflection of light rays through the fluid layer can be derived from Fermat's principle. Such a model would be useful if the temperature field is known throughout the fluid layer, such as in numerical solutions of a given convection problem (e.g. Arter 1985; Busse & Frick 1985 who consider square-planform convection). The appropriate equations are given in Merzkirch (1974) and Emrich (1981, part 2). The model proposed here is particularly simple and immediately applicable to the long-wavelength approximations.

The most striking representation of theoretical shadowgraphs is achieved when the light-intensity pattern is used to produce pictures that resemble actual shadowgraphs, using a laser printer capable of representing 33 different shades of grey. Each picture consists of a rectangular array of picture elements (pixels), each of which is assigned a shade of grey, assuming a logarithmic relationship between the light intensity and grey level, because both the human eye and photographic emulsion respond approximately logarithmically to light intensity. The pictures are scaled such that the brightest point is represented by a pure white pixel and the darkest spot by a pure black pixel. The similarity between the pictures and actual shadowgraphs is impressive and enlightening.

4. Results

The focusing height, $z = z_{\mathrm{F}}$, is the height at which converging light rays first intersect. At such a point, the Jacobian is zero, so the light intensity is infinite. In the theoretical shadowgraphs presented here, the focusing height is set so that the ratio of maximum to minimum light intensity is about 200, which avoids the problem of infinite intensity.

Figure 3(*a*) shows the theoretical shadowgraph for the roll planform, equation (2.5), over the range $-8\pi/a \leqslant x \leqslant 8\pi/a$. At a position just above the convecting layer, the variation in light intensity is small. But at $z = z_{\mathrm{F}}$ there is a large variation in light intensity. The sinusoidally varying temperature distribution is represented by sharp white lines separating large dark regions. The white lines correspond to vertical surfaces on which the temperature is a minimum, and correspondingly the vertical velocity component is directed downwards. Figure 3(*b*) shows a photograph of an actual shadowgraph of convection near onset in the form of rolls, observed by Busse & Whitehead (1971). The correspondence between the theoretical and experimental shadowgraphs is obvious.

Figure 4(*a*) shows the theoretical shadowgraph for the square planform, equation (2.6), over the range $-4\pi/a \leqslant x, y \leqslant 4\pi/a$. The temperature distribution in the convecting fluid is a chequerboard pattern, but once the light is focused, the picture consists of intersecting bright lines and large dark areas. Again, the bright lines are

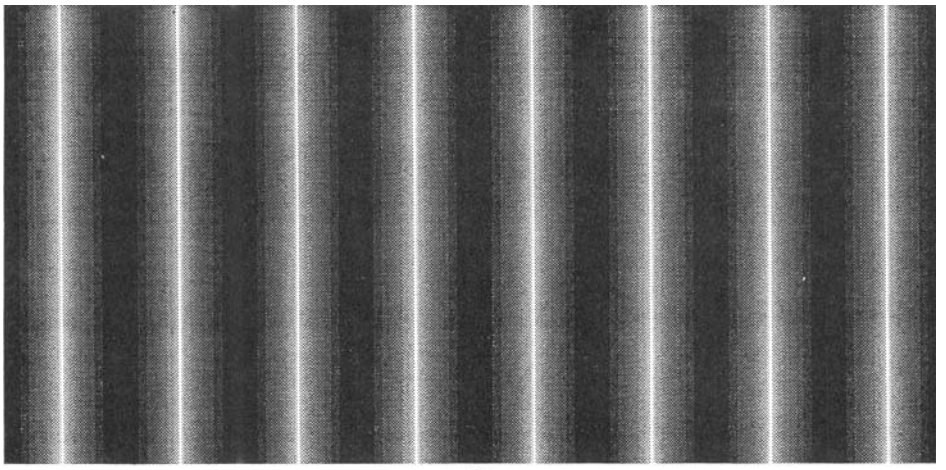

(*a*)

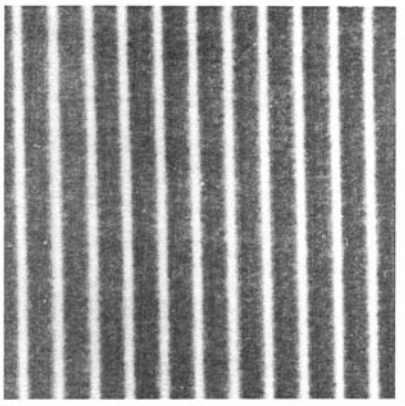

(*b*)

FIGURE 3. (*a*) Theoretical shadowgraph for roll-planform convection, equation (2.5). The picture is for the range $-8\pi/a \leqslant x \leqslant 8\pi/a$. (*b*) Experimentally observed shadowgraph for roll-planform convection near onset (from Busse & Whitehead 1971).

caused by the deflection of light rays towards the cold fluid, and they represent surfaces through which no fluid flows and the vertical velocity component is directed downwards (or is zero). A shadowgraph of convection near onset in the form of square cells, observed by Le Gal *et al.* (1985), is shown in figure 4(*b*). There is close correspondence between the experimental and theoretical shadowgraphs.

Figure 5(*a*) shows the theoretical shadowgraph for the hexagonal planform, equation (2.7), over the range $0 \leqslant x \leqslant 16\pi/\sqrt{3}a$, $-6\pi/a \leqslant y \leqslant 2\pi/a$. The shadowgraph is a series of bright lines, which constitute the cell boundaries of the hexagons. These are again surfaces through which no fluid flows and on which the vertical velocity component is directed downwards. Koschmieder & Biggerstaff (1986) obtained shadowgraphs of the onset of hexagonal convection in a thin fluid

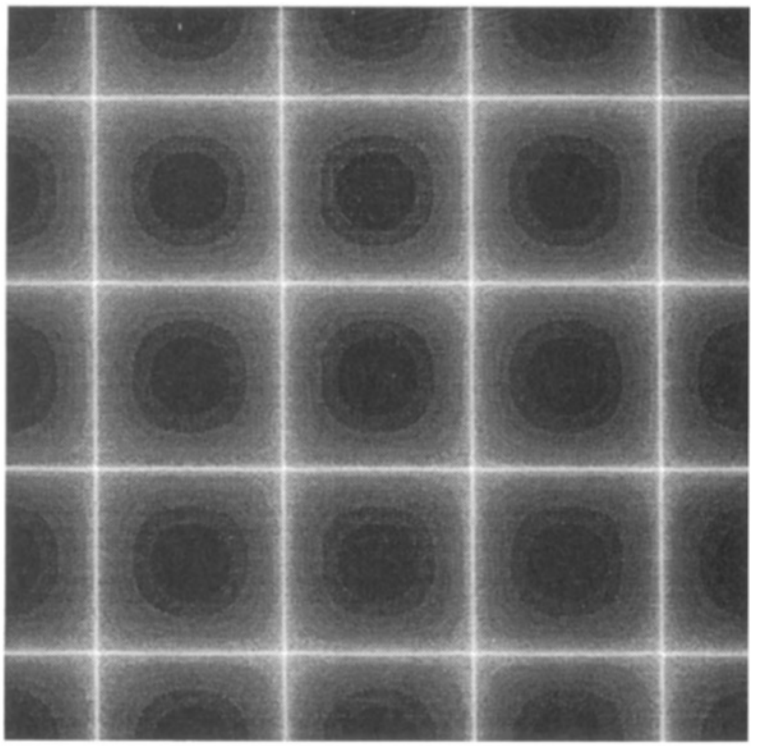

(a)

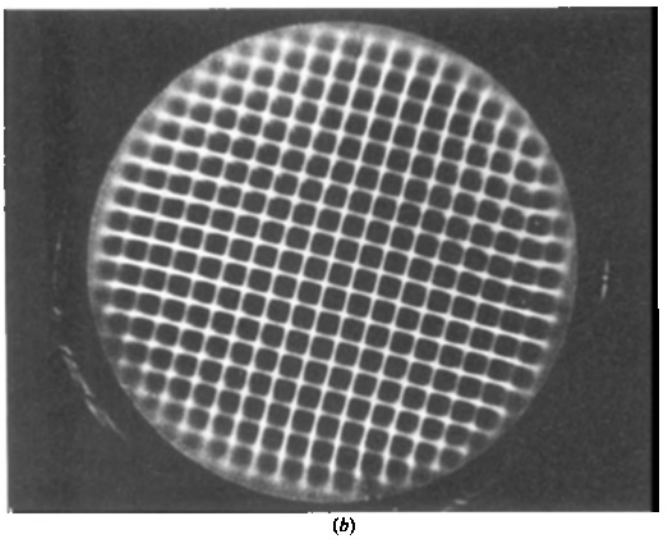

(b)

FIGURE 4. (a) Theoretical shadowgraph for square-planform convection, equation (2.6). The picture is for the range $-4\pi/a \leqslant x, y \leqslant 4\pi/a$. (b) Experimentally observed shadowgraph for square-planform convection near onset (from Le Gal *et al.* 1985).

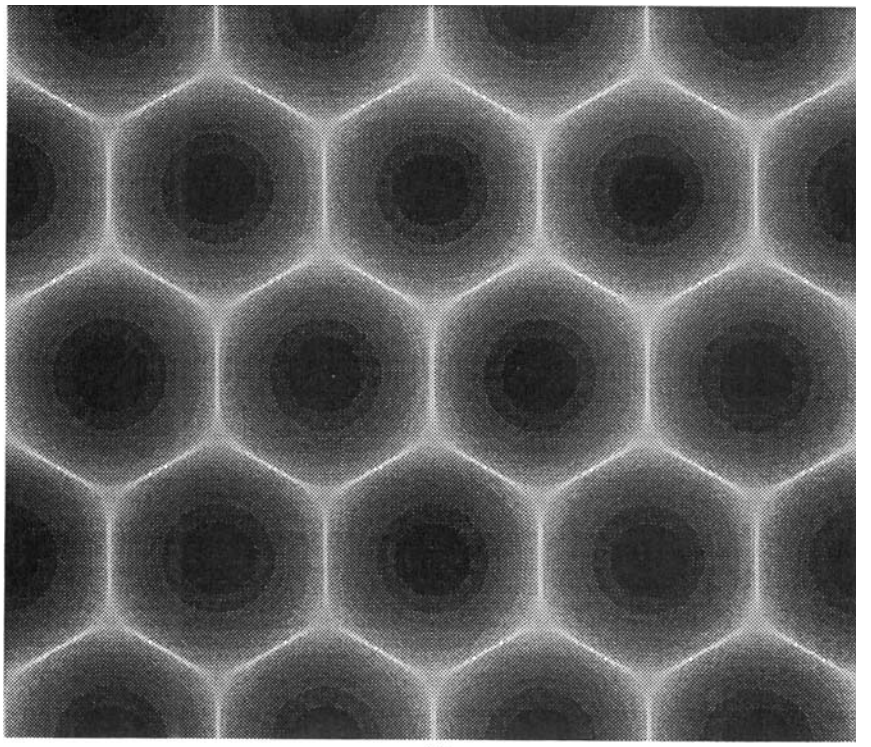

(*a*)

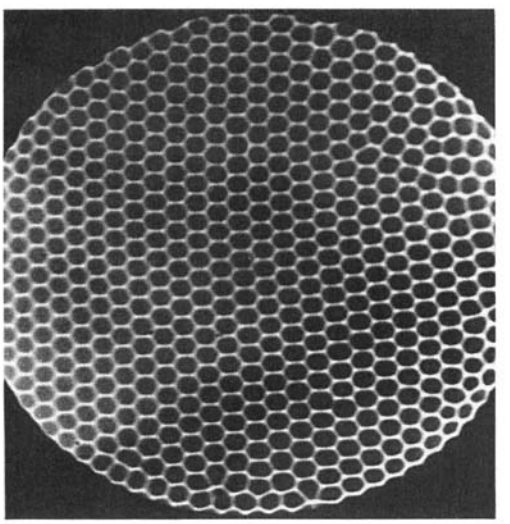

(*b*)

FIGURE 5. (*a*) Theoretical shadowgraph for ℓ-hexagonal-planform convection, equation (2.7). The picture is for the range $0 \leqslant x \leqslant 16\pi/\sqrt{3}a$, $-6\pi/a \leqslant y \leqslant 2\pi/a$. (*b*) Experimentally observed shadowgraph for hexagonal-planform convection near onset (from Koschmieder & Biggerstaff 1986).

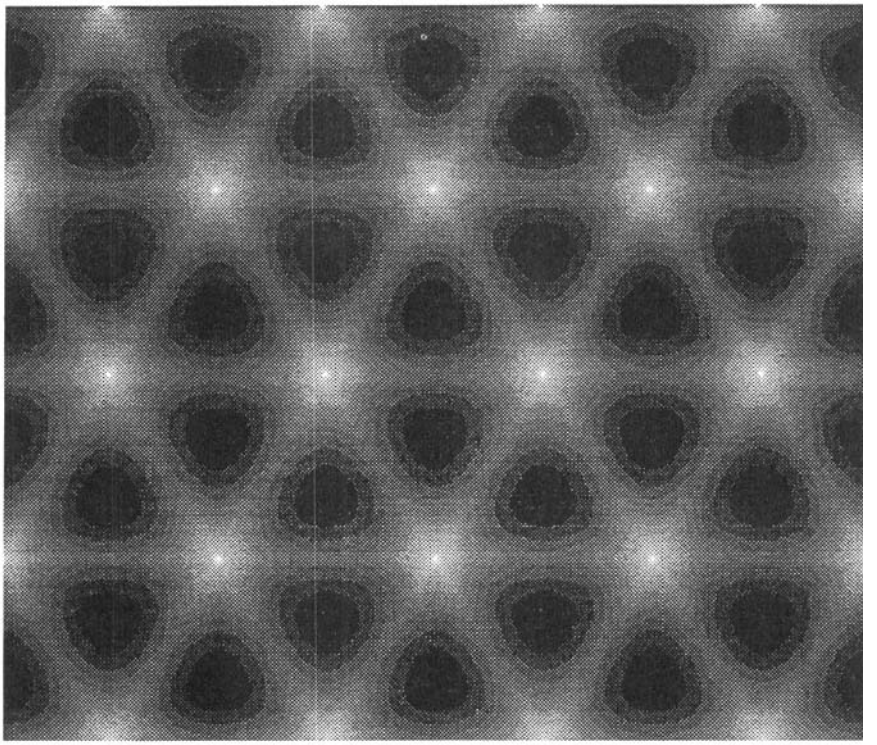

(a)

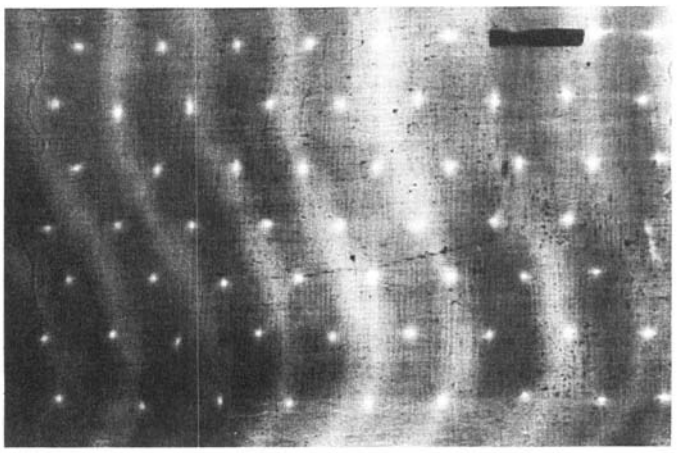

(b)

FIGURE 6. (a) Theoretical shadowgraph for g-hexagonal-planform convection, i.e. equation (2.7) multiplied by -1. (b) Experimentally observed shadowgraph for down-hexagonal convection (from Carrigan 1985). The wavy pattern is not associated with the flow field.

layer, and one such pattern is reproduced in figure 5(*b*). There is excellent correspondence between the theoretical and experimental shadowgraphs.

Changing the sign of f for the roll and square planforms results in the same shadowgraph pattern, translated by π/a in each direction. For the hexagonal planform, however, changing the sign of f produces an entirely different pattern, as shown in figure 6(*a*). The light rays are now focused at the centre of each hexagon, yielding an array of bright spots surrounded by dark patches. Figure 6(*b*) shows a shadowgraph produced by Carrigan (1985) in an experimental study of convection with internal heating. The two figures are very similar, indicating that fluid is flowing down at the centre of each hexagon and up along the edges of the cells, which are not visible. There is also the impression of bright regions joining each bright spot in figure 6, so the pattern resembles an array of equilateral triangles. Triangular patterns have been observed by White (1982), but the relationship with figure 6 is unclear. In the notation of Busse (1978), the shadowgraphs of figure 5 correspond to the ℓ-hexagon, commonly observed in liquids, while that of figure 6 corresponds to the g-hexagon, commonly observed in gases. The g-hexagon is called a down-hexagon by Carrigan, since he observed this form of convection in liquids with internal heating.

The significance of figures 3–6 is that we have provided a direct comparison of the shadowgraphs produced by theoretical expressions of linear theory with experiments of convection near onset, where linear effects dominate. We have shown that the square planform produces a shadowgraph comprising square cells, and that bright lines coincide with surfaces through which no fluid flows, and on which the vertical component of velocity is directed downwards (or is zero). The results confirm the ideas of Stuart (1964) for the hexagonal planform, but refute his suggestion that equation (2.6) for the square planform will not result in square cells. The ambiguity inherent in the square planform, under Stuart's definition of cellular boundaries, is removed because the focusing effect of shadowgraphs selects the downwards-flowing (and hence cold) surfaces.

The effect of the logarithmic filter applied to the light-intensity data is significant. Without it the square planform looks different because there are sharp peaks of light intensity at the corners of each cell, resulting in a square array of bright spots. However, as we are attempting to produce pictures that represent shadowgraphs, it is necessary to take account of all steps in the process, including the response of the viewing apparatus, whether it be eyes or a camera.

At Rayleigh numbers significantly above critical, the linear approximations represented by (2.3)–(2.7) will be modified by higher-order terms. We consider the shadowgraphs produced by a planform function of the form (2.9) derived from the long-wavelength equation (2.8). We emphasize that the examples presented are indicative of the effects of higher-order terms, but may be somewhat arbitrary. The parameters δ and ξ have been adjusted until a picture having certain desired features was obtained. Also, the form of f given here is only applicable to the poorly conducting-boundaries example.

Figure 7(*a*) shows a shadowgraph of the roll planform derived from (2.5), (2.10) and (2.11), with $\delta = 2.5$ and $\xi = 0.1$. There are additional bright bands due to higher-order terms, which creates the impression of a dark strip along the centre of each roll. Figure 7(*b*) shows a shadowgraph of roll cells by Busse & Whitehead (1971). This represents convection at a highly supercritical Rayleigh number, where nonlinear effects are significant. Even so, there is some resemblance between the theoretical and experimental shadowgraphs. Figure 8(*a*) shows a shadowgraph of the square

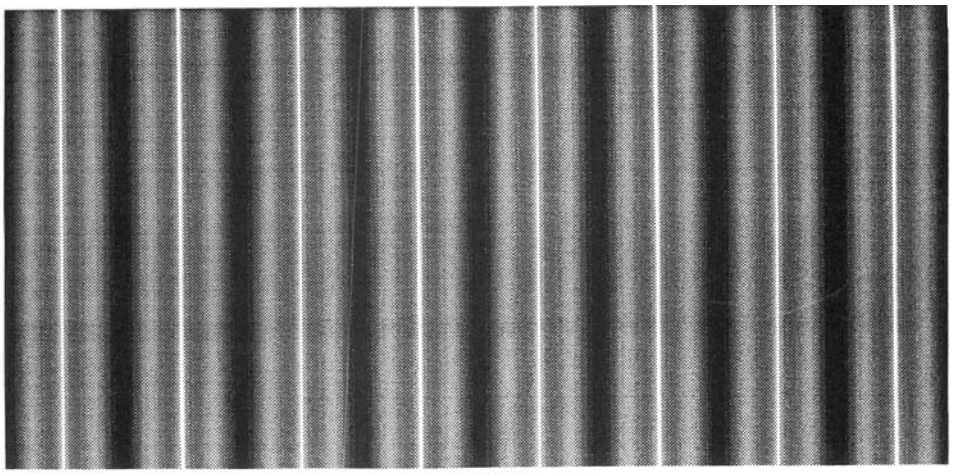

(a)

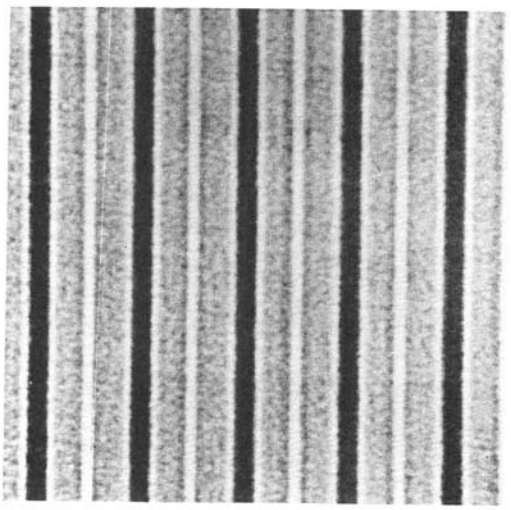

(b)

FIGURE 7. (a) Theoretical shadowgraph for roll-planform convection, including higher-order terms, with $\delta = 2.5$ and $\xi = 0.1$. (b) Experimentally observed shadowgraph for roll-planform convection at high Rayleigh number (from Busse & Whitehead 1971).

planform derived from (2.6), (2.10) and (2.11), with $\delta = 2.5$ and $\xi = 0.1$. The square cell remains almost intact, but the combination of higher-order terms has produced a dark spot in the centre of each cell surrounded by a halo. The result is reminiscent of the cell interiors observed by White (1982), such as in the shadowgraph shown in figure 8(b). This shadowgraph represents highly supercritical convection, where again the effects of nonlinearities are significant. Such a result could only be obtained with non-zero ξ, so that f_2 was non-zero, which suggests that the dark-spot effect is due primarily to the temperature dependence of viscosity. Figure 9 shows a

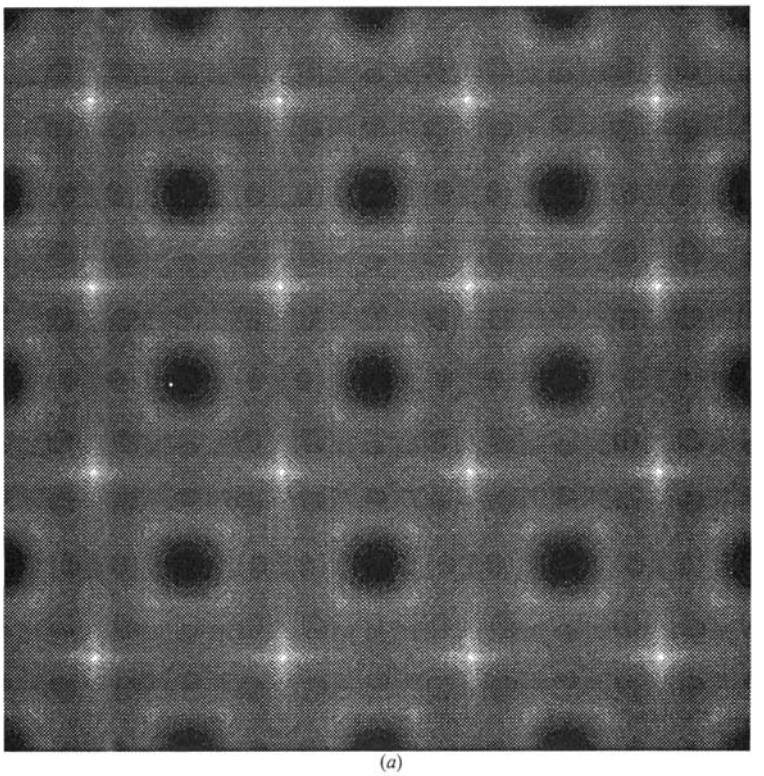

(*a*)

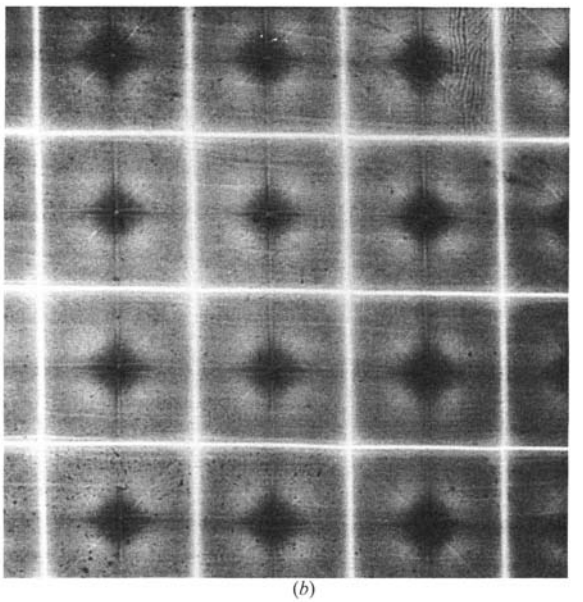

(*b*)

FIGURE 8. (*a*) Theoretical shadowgraph for square-planform convection, including higher-order terms, with $\delta = 2.5$ and $\xi = 0.1$. (*b*) Experimentally observed shadowgraph for square-planform convection at high Rayleigh number (from White 1982).

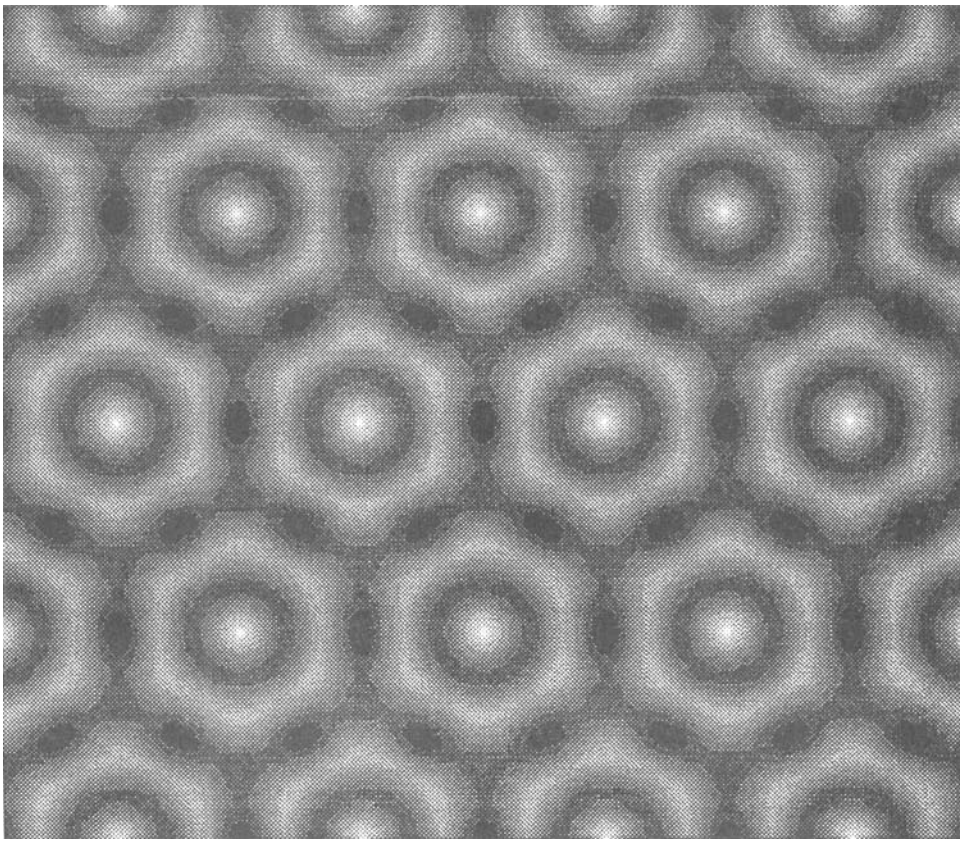

FIGURE 9. Theoretical shadowgraph for ℓ-hexagonal-planform convection, including higher-order terms, with $\delta = 2.5$ and $\xi = 0.1$.

shadowgraph of an ℓ-hexagon derived from (2.7), (2.11)–(2.13), with $\delta = 2.5$ and $\xi = 0.1$. Again the combination of linear and higher-order terms has produced a cell that has a dark spot in the centre surrounded by a brighter region, also reminiscent of experimental results. Figure 10 shows a shadowgraph of a g-hexagon derived from (2.7), (2.11)–(2.13), with $\delta = -2.5$ and $\xi = 0.1$. The effect of the higher-order terms this time is to produce hexagonal haloes around each bright spot. The triangular image of the linear shadowgraph has disappeared.

Another convection planform sometimes observed in convection experiments (see for example Busse & Whitehead 1974) is the bimodal planform. It is essentially the superposition of a set of rolls of small amplitude and large wavenumber perpendicular to a dominant set of rolls. The discrepancy in wavenumbers between the two sets of rolls results in a rectangular-cell structure. The bimodal planform is a high-Rayleigh-number phenomenon, so it would be difficult to generate an accurate shadowgraph using the approach presented here. As an example, we present the shadowgraph of figure 11(*a*), which was obtained from the planform function

$$f = \cos ax + 0.2 \cos 1.5ax. \tag{4.1}$$

The shadowgraph in figure 11(*b*) is from an experiment by Busse & Whitehead

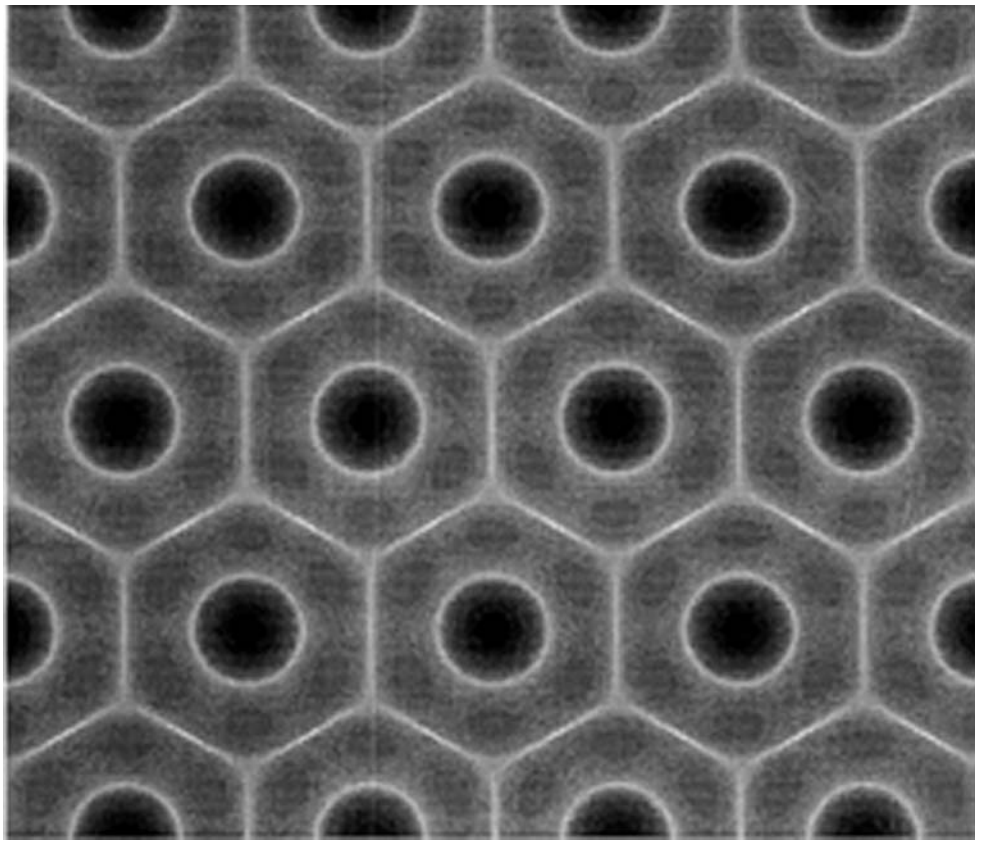

FIGURE 10. Theoretical shadowgraph for g-hexagonal-planform convection, including higher-order terms, with $\delta = -2.5$ and $\xi = 0.1$.

(1974). The two figures do not compare particularly well, probably because (4.1) is not an accurate representation of the flow.

Another effect to consider in the production of shadowgraphs is *caustics*. These are observed when the screen is placed at a point past the focusing plane. At such a point, some light rays have intersected and the result is that discontinuities exist in the intensity field. As an example, we present a theoretical shadowgraph for the roll planform of figure 7(*a*), but at approximately 10 times the focusing height, z_F. The result, shown in figure 12, resembles figure 7(*b*), indicating that caustics may occur in the experimental result. The discontinuity in intensity (i.e. the caustic) results in clearly defined dark regions separating light bands, with bright lines at the centre. For high-Rayleigh-number flows, the focusing height may be much smaller than for flows near onset (since the deflection through the layer, and hence K, ought to be greater), so it is easily understood how caustics may be apparent in shadowgraphs. The existence of caustics makes the interpretation of shadowgraphs more difficult.

5. Conclusions

The following points are evident from this study.

(i) A shadowgraph is not simply a vertical average of the temperature field in a

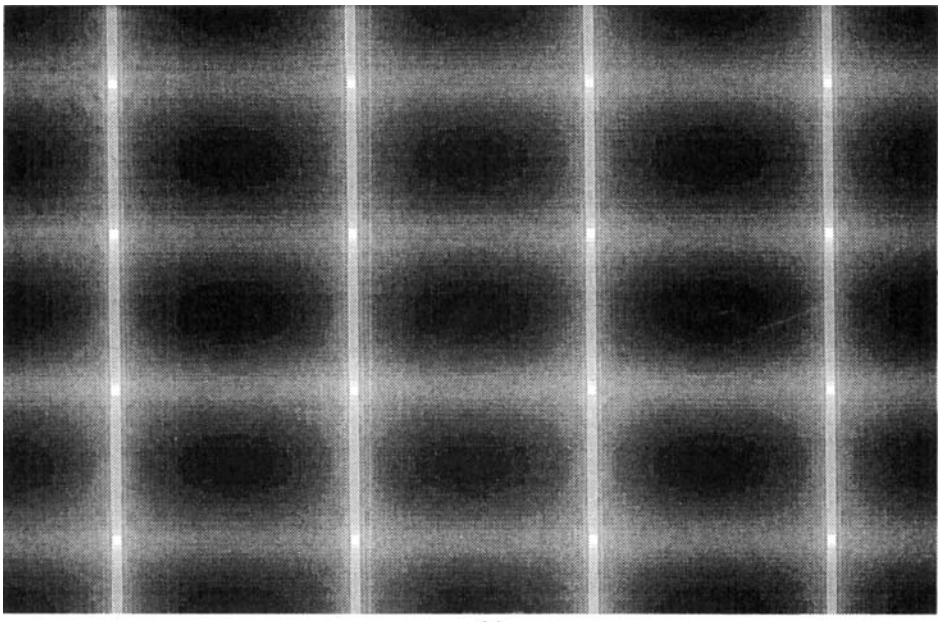

(a)

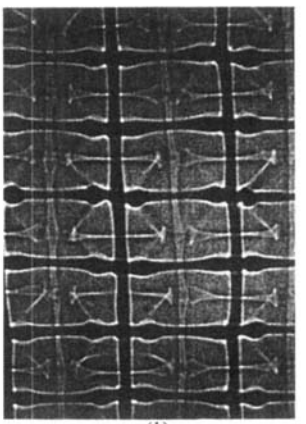

(b)

FIGURE 11. (a) Theoretical shadowgraph for bimodal convection, equation (4.1). The picture is for the range $-4\pi/a \leqslant x \leqslant 4\pi/a$, $-8\pi/3a \leqslant y \leqslant 8\pi/3a$. (b) Experimentally observed shadowgraph for bimodal convection (from Busse & Whitehead 1974).

convecting fluid, owing to the effect of focusing of light rays above the fluid layer and the possibility of caustics.

(ii) When the temperature field takes the form of a roll, square or hexagonal planform of linear theory, the shadowgraph comprises bright lines along the edge of each cell and cell interiors of almost uniform light intensity. The bright lines correspond to surfaces through which no fluid flows and on which the vertical component of velocity is directed *downwards*. The effect of focusing in the

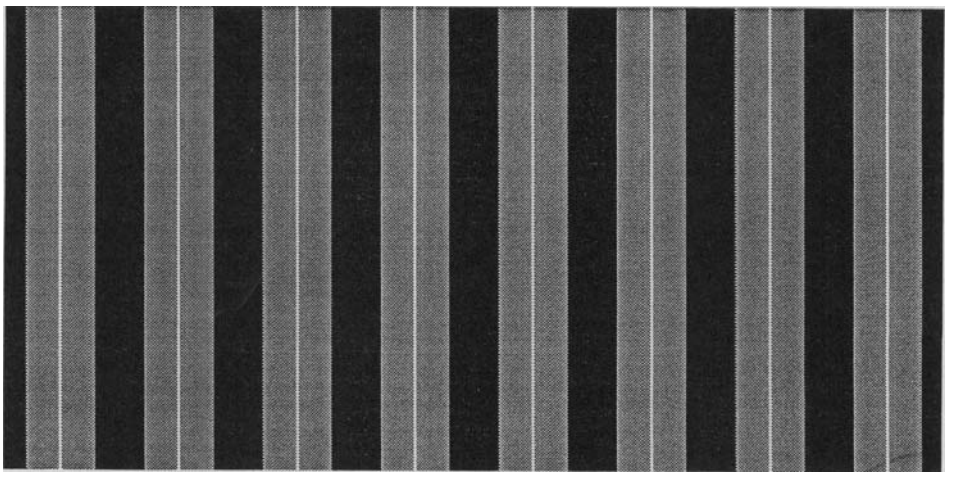

FIGURE 12. Theoretical shadowgraph for roll-planform convection, with $\delta = 2.5$ and $\xi = 0.1$, at approximately 10 times the focusing height.

shadowgraph process is to remove the ambiguity in the definition of square cell boundaries, as suggested by Stuart (1964).

(iii) Experimental studies of convection near onset by Busse & Whitehead (1971), Le Gal *et al.* (1985) and Koschmieder & Biggerstaff (1986) have produced shadowgraphs of roll, square and hexagonal cells, respectively, which are very similar to the shadowgraphs produced here using only linear terms.

(iv) There is no dark spot at the centre of a hexagonal cell, corresponding to the upward fluid motion there. The dark spot is a higher-order effect. Similarly, there is no dark line at the centre of a roll cell.

(v) The dark-spot effect can be produced by adding higher-order terms to the planform function for each of the roll, square or hexagonal planforms. The effect is generally observed at highly supercritical Rayleigh numbers, where the linear form is significantly modified.

(vi) Modelling of the shadowgraph process is a useful tool for prediction of experimentally observed shadowgraph patterns corresponding to theoretically or computationally derived convection planforms. In particular, it should be valuable for comparison of numerical studies of three-dimensional convection, such as those by Arter (1985), Frick, Busse & Clever (1983) and Busse & Frick (1985), with actual observations. The amount of computation required for determining the shadowgraphs ought to be small compared with that necessary for generating the numerical solutions.

Finally, we note that the square planform proposed by Drobyshevski & Yuferev (1974), in order to give the same topology as a hexagon, is essentially just the second-order terms, f_2, given by (2.11*a*). Such a form alone could not produce shadowgraphs comparable with those observed.

The author wishes to acknowledge much helpful discussion with A. J. Bernoff, A. N. Ellis and J. W. Swift, of DAMTP, University of Cambridge, where part of this work was done. Financial support for my time in Cambridge was provided by the Commonwealth Scholarships and Fellowships Plan. I also thank A. J. Baddeley and M. J. Buckley of CSIRO DMS for providing software to process and produce the

shadowgraph pictures. I am grateful to Drs C. R. Carrigan, E. L. Koschmieder, P. Le Gal, D. White and J. A. Whitehead for providing me with photographs of their experimental work and for permission to reproduce them.

REFERENCES

ARTER, W. 1985 Nonlinear Rayleigh–Bénard convection with square planform. *J. Fluid Mech.* **152**, 391–418.

BUSSE, F. H. 1978 Nonlinear properties of thermal convection. *Rep. Prog. Phys.* **41**, 1929–1967.

BUSSE, F. H. & FRICK, H. 1985 Square-pattern convection in fluids with strongly temperature-dependent viscosity. *J. Fluid Mech.* **150**, 451–465.

BUSSE, F. H. & RIAHI, N. 1980 Nonlinear convection in a layer with nearly insulating boundaries. *J. Fluid Mech.* **96**, 243–256.

BUSSE, F. H. & WHITEHEAD, J. A. 1971 Instabilities of convection rolls in a high Prandtl number fluid. *J. Fluid Mech.* **47**, 305–320.

BUSSE, F. H. & WHITEHEAD, J. A. 1974 Oscillatory and collective instabilities in large Prandtl number convection. *J. Fluid Mech.* **66**, 67–79.

CARRIGAN, C. R. 1985 Convection in an internally heated, high Prandtl number fluid: A laboratory study. *Geophys. Astrophys. Fluid Dyn.* **32**, 1–21.

CHAPMAN, C. J. & PROCTOR, M. R. E. 1980 Nonlinear Rayleigh–Bénard convection between poorly conducting boundaries. *J. Fluid Mech.* **101**, 759–782.

DEPASSIER, M. C. & SPIEGEL, E. A. 1982 Convection with heat flux prescribed on the boundaries of the system. I. The effect of temperature dependence of material properties. *Geophys. Astrophys. Fluid Dyn.* **21**, 167–188.

DROBYSHEVSKI, E. M. & YUFEREV, V. S. 1974 Topological pumping of magnetic flux by three-dimensional convection. *J. Fluid Mech.* **65**, 33–44.

EMRICH, R. J. (ed.) 1981 *Methods of Experimental Physics, vol. 18A – Fluid Dynamics.* Academic.

FRICK, H., BUSSE, F. H. & CLEVER, R. M. 1983 Steady three-dimensional convection at high Prandtl numbers. *J. Fluid Mech.* **127**, 141–153.

GERTSBERG, V. L. & SIVASHINSKY, G. I. 1981 Large cells in nonlinear Rayleigh–Benárd convection. *Prog. Theor. Phys.* **66**, 1219–1229.

HOUSEMAN, G. 1981 Numerical experiments on mantle convection. Ph.D. dissertation, University of Cambridge.

JENKINS, D. R. 1987 Rolls versus squares in thermal convection of fluids with temperature-dependent viscosity. *J. Fluid Mech.* **178**, 491–506.

JENKINS, D. R. & PROCTOR, M. R. E. 1984 The transition from roll to square-cell solutions in Rayleigh–Bénard convection. *J. Fluid Mech.* **139**, 461–471.

KOSCHMIEDER, E. L. 1966 On convection on a uniformly heated plane. *Beitr. Z. Phys. Atmos.* **39**, 1–11.

KOSCHMIEDER, E. L. & BIGGERSTAFF, M. I. 1986 Onset of surface-tension-driven Bénard convection. *J. Fluid Mech.* **167**, 49–64.

LE GAL, P., POCHEAU, A. & CROQUETTE, V. 1985 Square versus roll pattern at convective threshold. *Phys. Rev. Lett.* **54**, 2501–2504.

MERZKIRCH, W. 1974 *Flow Visualization.* Academic.

OLIVER, D. S. & BOOKER, J. R. 1983 Planform of convection with strongly temperature dependent viscosity. *Geophys. Astrophys. Fluid Dyn.* **27**, 73–85.

PROCTOR, M. R. E. 1981 Planform selection by finite-amplitude thermal convection between poorly conducting slabs. *J. Fluid Mech.* **113**, 469–485.

RYRIE, S. C. 1987 The scattering of light by a chaotically convecting fluid. *J. Fluid Mech.* **174**, 155–185.

SCHMIDT, H. U., SIMON, G. W. & WEISS, N. O. 1985 Buoyant magnetic flux tubes. II. Three-dimensional behaviour in granules and supergranules. *Astron. Astrophys.* **148**, 191–206.

STUART, J. T. 1964 On the cellular patterns in thermal convection. *J. Fluid Mech.* **18**, 481–498.

SWIFT, J. W. 1984 Bifurcation and symmetry in convection. Ph.D. dissertation, University of California, Berkeley.

WHITE, D. B. 1982 Experiments with convection in a variable viscosity fluid. Ph.D. dissertation, University of Cambridge.

WHITEHEAD, J. A. & PARSONS, B. 1978 Observations of convection at Rayleigh numbers up to 760,000 in a fluid with large Prandtl number. *Geophys. Astrophys. Fluid Dyn.* **9**, 201–217.